



OPEN ACCESS

EDITED BY
Iskander Tlili,
Tunisia

REVIEWED BY
Rizwan Ul Haq,
Bahria University, Pakistan
A. Mahdy,
South Valley University, Egypt

*CORRESPONDENCE
Huda Alfannakh,
halfannakh@kfu.edu.sa

SPECIALTY SECTION
This article was submitted to Process
and Energy Systems Engineering,
a section of the journal
Frontiers in Energy Research

RECEIVED 03 May 2022
ACCEPTED 11 July 2022
PUBLISHED 09 August 2022

CITATION
Alfannakh H (2022), Significances of
magnetic dipole flow and melting heat
transfer over suspended dust particles
along with carbon nanotubes.
Front. Energy Res. 10:935108.
doi: 10.3389/fenrg.2022.935108

COPYRIGHT
© 2022 Alfannakh. This is an open-
access article distributed under the
terms of the [Creative Commons
Attribution License \(CC BY\)](#). The use,
distribution or reproduction in other
forums is permitted, provided the
original author(s) and the copyright
owner(s) are credited and that the
original publication in this journal is
cited, in accordance with accepted
academic practice. No use, distribution
or reproduction is permitted which does
not comply with these terms.

Significances of magnetic dipole flow and melting heat transfer over suspended dust particles along with carbon nanotubes

Huda Alfannakh*

Department of Physics, College of Science, King Faisal University, Al-Ahsa, Saudi Arabia

The current research letter is materialized to examine the combined effect of thermophoretic dust particle diffusion and magnetic dipole flow toward a stretchable sheet. The slip effect is used in the development of the momentum equation. Water is considered as a base fluid, and single-walled carbon nanotubes and multiwalled carbon nanotubes are nanoparticles. The aforementioned rheological model is formulated in the way of nonlinear partial differential equations (PDEs). The structure of nonlinear bifurcated ordinary differential equations (ODEs) is obtained from the modeled nonlinear PDEs by incorporating valid sameness transformations. The system of ODEs is then figured out by employing the tool of MATLAB function `bvp4c`. The significant nature of the contributing parameter for both the single-wall and multiwall cases is presented via graphs. From the results, we conclude that an impact of the melting effect, mounting of Pr , reported a thinner thermal boundary layer thickness. Furthermore, a clear rise of nanofluid temperature is noticed for the greater melting M_1 parameter. The slip parameter plays a significant role in the enhancement of the velocity profile.

KEYWORDS

melting surface, magnetic dipole, carbon nanotubes, slip flow, numerical analysis

Introduction

Nanofluids may be used to improve the performance of different electronic and mechanical devices regarding heat transfer due to their high thermal conductivity. Therefore, researchers have suggested many proposals to upgrade the capability of transfer of heat in the fluids. Nanofluids are an advanced way to enhance the heat-transfer rate in liquids. They contain nanoparticles homogeneously dissolved in simple fluids, for example, oil, water, and glycerin. There are many kinds of nanoparticles, such as aluminum, silver, gold, titanium, copper, the oxides of these metals, and carbon nanotubes. These fluids have several applications in industries, like vehicle cooling, heat exchangers, electronic cooling, nuclear reactors, cooling thermal insulation, cancer therapy, energy production, and so on.

Moreover, nanofluids have several applications, like micromachines in microreactors, cars, computer chips, microelectronics, and cooling agents in aeroplanes. Nanofluid

properties may depend on different parameters such as particle dimension, particle distribution, shapes, size, and so on. Choi, 1995 was the first to observe that adding nanoparticles to a host fluid boosts its thermic strength. Later, Choi et al., 2001 showed through experiments that the enhancement in fluid thermic strength could also be achieved by taking oil as the base fluid. After the pioneering work of Choi, several scientists start working on nanofluids. Sheikholeslami et al., 2018 examined the nanofluid flow over a permeable channel in addition to Lorentz forces. Chen et al., 2015 inspected the nanofluid flow over a vertical symmetrical heated parallel plate with magnetic effects. Hayat and Nadeem, 2017 collectively worked on silver and copper oxide-based hybrid nanofluids to boost the heat-transfer rate. Dogonchi and Ganji (Dogonchi and Ganji, 2016) discussed the thermal radiation effect and flow of magnetohydrodynamic nanofluids between the contracting walls. Bilal et al. (Bilal et al., 2018) investigated the nanofluid flow across the contracting cylinder. Hayat et al., 2016 hypothesized the stagnation point flow with mass flux and variable heat conductivity, where a linear stretched surface subordinates the flow. Recent studies regarding the slip motion can be found in Rizwan Ul Haq et al., 2017; Ul Haq et al., 2018; Rizwan et al., 2020; and Ul Haq et al., 2020.

In the presence of an electrically conducting fluid, the phenomenon is called magnetohydrodynamics (MHD) when the magnetic field is applied across the moving fluid. MHD plays an essential role in many technological and industrial sectors such as nuclear fuels, cancer tumor treatment, blood pump machines, MHD generators, flow meters, and accelerator pumps. In the existence of the magnetic field, convection problems of the electrically conducting fluid have significant results because of its broad uses in astrophysics, missile technology, geophysics, and plasma physics. It is also frequently used in biomedicine industries. It is noticed that the combined impact of thermal radiation and MHD is an essential factor in the study of fluid dynamics owing to their extensive applications in furnace design, nuclear reactor safety, fire spreads, glass production, modern energy transformation devices, turbid water bodies, natural gas-fired and open cycle coal, photochemical reactors, natural convection in cavities, and many others. Metallurgy industries, petroleum, and chemical engineering are some specific processes where the importance of MHD along with thermal radiation can be observed. Qayyum et al. (Fakour et al., 2015) examined the nonlinear chemical reactions in MHD flow above the stretched sheet having a variable thickness. They also examined heat absorption/generation and nonlinear convection. Pourmehran et al. (Qayyum et al., 2017) considered the bouncy effects bygone a vertical sheet for investigating the MHD convective nanofluid. Shiekholeslami (Mahanthesh et al., 2017) used the Lattice Boltzmann technique as a mesoscopic methodology to inspect the convective flow of MHD nanofluids in a porous cubic container. Zhao et al. (Pourmehran et al., 2016) focused on

the thermally generated flow of a nanofluid (water) through porous nanotubes and discussed heat-transfer features. Hayat et al., 2018 designed the magnetic-micropolar flow transverse to a curved stretching surface with homogeneous/heterogeneous interactions through an analytical technique. Khan et al. (Sheikholeslami, 2017) explained the flow of an unsteady MHD Newtonian fluid with coupled mass and heat transfer where wall shear stress is applied to the fluid. Using the vertical microchannel having conducting and non-conducting walls, Jha and Aina (Zhao et al., 2019) focused on studying applied and induced magnetic fields and natural convective flow. Hayat et al. (Hayat et al., 2017a) investigated the fluid flow rate in the existence of thermal surface boundary conditions. Hashemi et al. (Reddy et al., 2018) discussed the dynamics of a micropolar nanofluid in a radiative porous medium coupled with MHD natural convection and incorporation of an elliptical heat source. Alkanhal et al. (Alkanhal et al., 2019) studied the thermal management of MHD nanofluids within a porous medium enclosed in a wavy shaped cavity with a square obstacle in the presence of a radiation heat source. M.G. Reddy et al. (Reddy et al., 2022) discussed the effect of thermal conductivity on Blasius-Rayleigh-Stokes flow and heat transfer over a moving plate by considering the magnetic dipole moment.

The no-slip condition is also an essential part of Navier Stoke's equations. For most of the non-Newtonian fluids, the no-slip condition is inadequate as few polymers melt frequently, showing the microscopic wall slip, which has a modulating impact and has a nonlinear relationship between traction and slip velocity. Partial velocity slip occurs when the liquid flows over the polish surface or through different processes such as suspension, emulsions, polymer solutions, and foams. The Navier velocity slip condition has typical importance while observing the slip phenomena. Solutal slip and thermal slip conditions may also appear in different industrial procedures. The boundary layer slip flow problem occurs in internal cavities and the polishing of heart valves. Many researchers and scientists have investigated the behavior of flow under no-slip conditions. However, in real-life applications, it is not mandatory in every case because there are different circumstances in which velocities of body and fluid particles are distinct. The behavior of flow in microstructures/nanostructures such as hard drives, microvalves, micropumps, and micronozzles is indicated by the slip boundary conditions. Recent studies regarding the slip motion can be found in Hayat et al., 2013; Mukhopadhyay, 2013; Shen et al., 2015; Hayat et al., 2017b; Ul Haq et al., 2017; Hashemi et al., 2018; and Hayat et al., 2019.

This article examines the magnetic dipole flow and melting heat transfer over suspended dust particles with carbon nanotubes and the slip effect. To compose a nanofluid, the water base fluid is mixed up with two types of carbon nanotubes [single-walled carbon nanotubes (SWCNTs) and multiwalled carbon nanotubes (MWCNTs)]. By applying

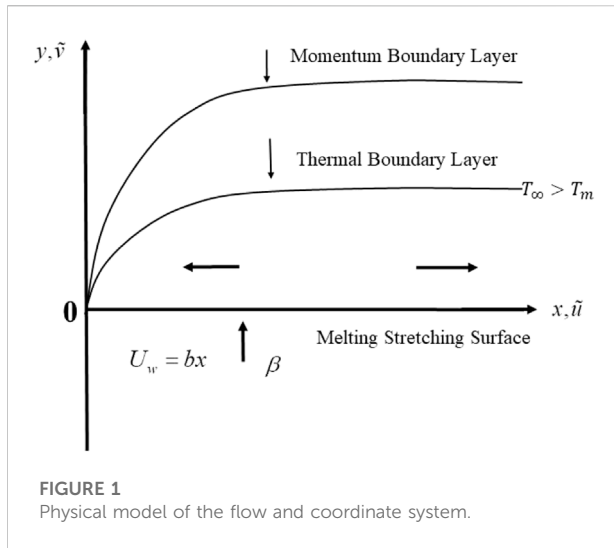


FIGURE 1 Physical model of the flow and coordinate system.

TABLE 1 Comparison of present numerical results with previous ones.

β	Ramesh et al., 2012	Present result
1	-1.41421	-1.4143
5	-2.44948	-2.4495
10	-3.31662	-3.3166
50	-7.14142	-7.1414

significant similarity transformation, nonlinear partial differential equations (PDEs) are being modified into a system of ordinary differential equations (ODEs); employing the MATLAB function bvp4c, we were able to get numerical solutions to these nonlinear ordinary differential equations. Tables and graphs are used to demonstrate the impact of different physical characteristics.

Mathematical formulation

Presumptions of the flow:

- Assume the 2D flow of dusty carbon nanotubes in an elaborated sheet where the flow is time-reliant as considered.
- $U_w(x) = bx$ is the velocity of the stretched sheet, where the stretching rate is $b > 0$ (Figure 1).
- The stretching surface as measured with the x -coordinate.
- The fluid utilized here is a dusty base fluid with the composition of water and carbon nanotubes (SWCNT/MWCNT).
- Equilibrium is assumed to be established between carbon nanotubes and the dust base fluid and the slip amid them.

TABLE 2 Thermophysical properties of water and nanotubes (Reddy and Kumar, 2021).

	ρ	c_p	k
Water	997.1	4,179	0.613
SWCNTs	2,600	425	6,600
MWCNTs	1,600	796	3,000

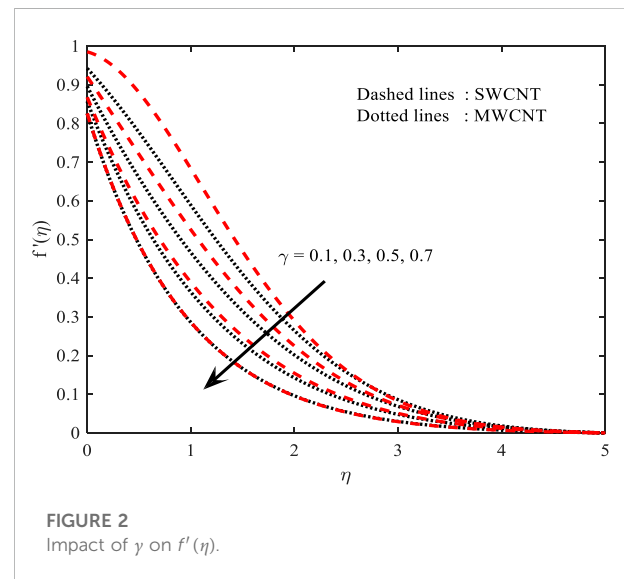


FIGURE 2 Impact of γ on $f'(\eta)$.

- The magnetic dipole field induced is ignored as the Reynolds number assumed is the least.

After using boundary layer approximation Bernoulli's equation in the free stream, the system of governing equations in the form of PDEs is as follows (Ramesh et al., 2012; Kumar et al., 2019):

Fluid phase

$$\frac{\partial \tilde{u}}{\partial x} + \frac{\partial \tilde{v}}{\partial y} = 0, \tag{1}$$

$$\tilde{u} \frac{\partial \tilde{u}}{\partial x} + \tilde{v} \frac{\partial \tilde{v}}{\partial y} = \frac{\mu_{nf}}{\rho_{nf}} \frac{\partial^2 \tilde{u}}{\partial y^2} + \frac{KN}{\rho_{nf}} (\tilde{u}_p - \tilde{u}) - \frac{\lambda_0 M}{\rho_{nf}} \frac{\partial H}{\partial x}, \tag{2}$$

$$\begin{aligned} & (\rho c_p)_{nf} \left[\tilde{u} \frac{\partial T}{\partial x} + \tilde{v} \frac{\partial T}{\partial y} \right] \\ & = k_{nf} \frac{\partial^2 T}{\partial y^2} + \frac{N c_{pf}}{\tau_t} (T_p - T) + \frac{N}{\tau_v} (\tilde{u}_p - \tilde{u})^2 - \left[\tilde{u} \frac{\partial H}{\partial x} \right. \\ & \left. + \tilde{v} \frac{\partial H}{\partial y} \right] \mu_f \lambda_0 T \frac{\partial M}{\partial T}, \end{aligned} \tag{3}$$

TABLE 3 Numerical values of $Re_x^{1/2}C_f$ and $Re_x^{1/2}Nu_x$ for various parameters.

β	ϕ	A	β_v	M_1	Pr	β_t	γ	Skin Friction		Nusselt number	
								SWCNT	MWCNT	SWCNT	MWCNT
0.1								1.882048	0.856694	0.101231	0.16372
0.2								1.890186	0.870788	0.100871	0.162767
0.3								1.898222	0.884311	0.100517	0.161827
	0.1							0.866065	0.87078	0.113392	0.162767
	0.2							1.245951	1.220881	0.107787	0.159973
	0.3							1.890186	1.605416	0.100871	0.039418
		0.1						3.727786	1.50517	0.112381	0.171434
		0.3						2.654772	1.156917	0.106464	0.167443
		0.5						2.086949	0.94767	0.102465	0.164201
			0.1					1.883817	0.845717	0.102060	0.166032
			0.3					1.888740	0.864956	0.101163	0.163568
			0.5					1.891211	0.875054	0.100642	0.162137
				0.5				1.888452	0.847668	0.098280	0.131615
				1.0				1.897058	0.864393	0.110842	0.155303
				1.5				1.905507	0.880089	0.122443	0.172535
					1.0			1.890186	0.870788	0.083408	0.052772
					2.0			1.890186	0.870788	0.105127	0.063023
					3.0			1.890186	0.870788	0.125422	0.072492
						0.5		1.890186	0.870788	0.10148	0.115659
						1.0		1.890186	0.870788	0.102426	0.131291
						1.5		1.890186	0.870788	0.102604	0.142206
							1.0	1.890186	0.870788	0.103929	0.236498
							2.0	1.890186	0.870788	0.090252	0.222124
							3.0	1.890186	0.870788	0.079756	0.209397

Dust phase

$$\frac{\partial \tilde{u}_p}{\partial x} + \frac{\partial \tilde{v}_p}{\partial y} = 0, \tag{4}$$

$$\tilde{u}_p \frac{\partial \tilde{u}_p}{\partial x} + \tilde{v}_p \frac{\partial \tilde{u}_p}{\partial y} = \frac{K}{m} (\tilde{u} - \tilde{u}_p) \tag{5}$$

$$\tilde{u}_p \frac{\partial T_p}{\partial x} + \tilde{v}_p \frac{\partial T_p}{\partial y} = \frac{c_{pf}}{c_{mf} T_t} (T - T_p) \tag{6}$$

The corresponding boundary conditions are given by

$$\tilde{u} = U_w + k_1 \frac{\partial \tilde{u}}{\partial y}, v = 0, T = T_m \text{ at } y = 0,$$

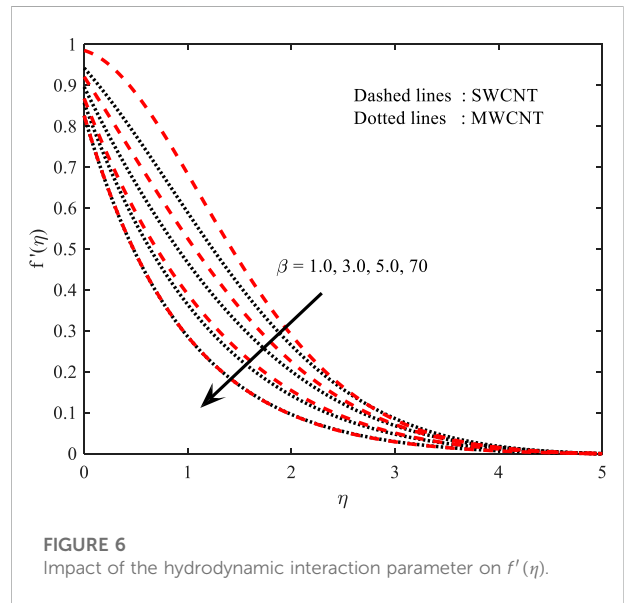
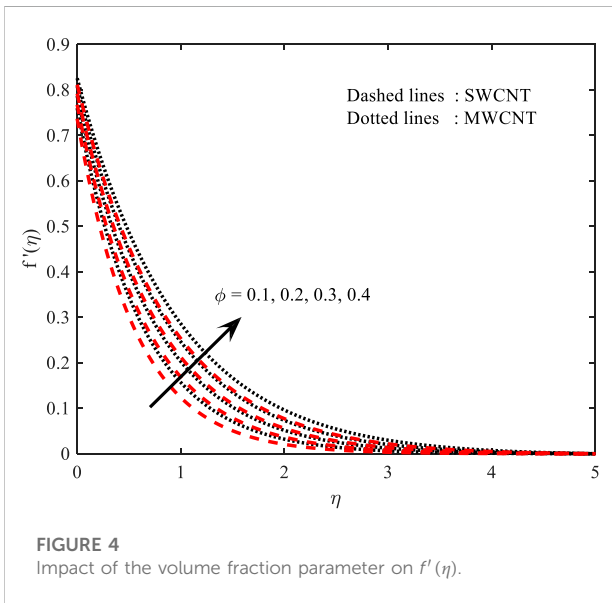
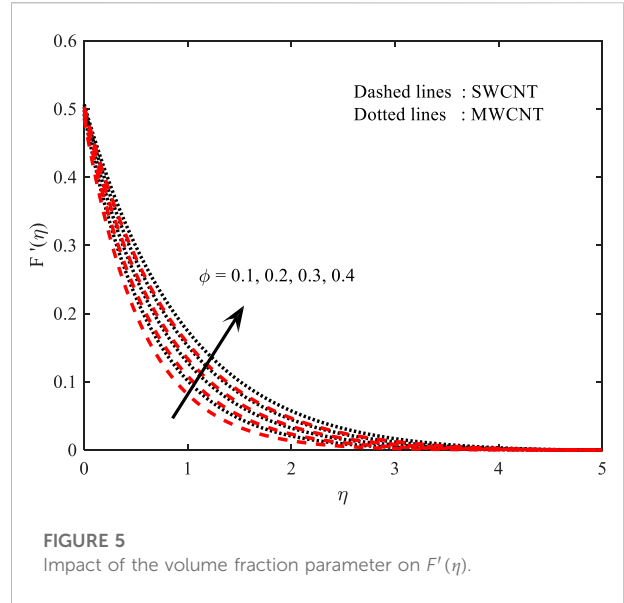
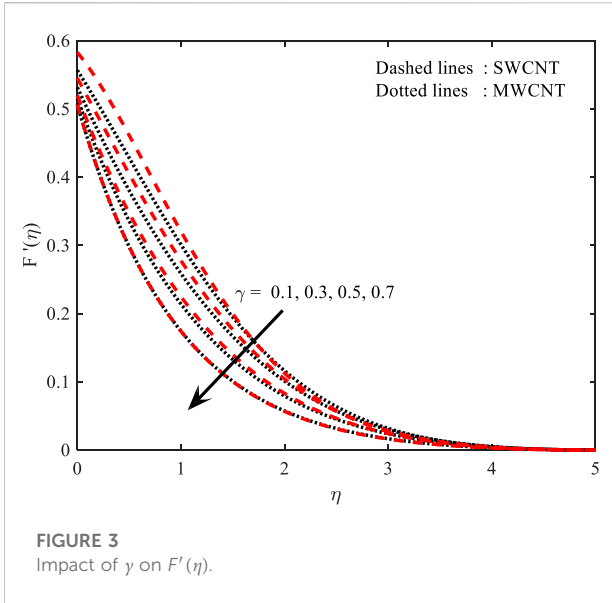
$$\tilde{u} \rightarrow 0, \tilde{u}_p \rightarrow 0, \tilde{v}_p \rightarrow \tilde{v}, T \rightarrow T_m, T_p \rightarrow T_\infty \text{ as } y \rightarrow \infty. \tag{7}$$

The expressions for viscosity, density, specific heat, and thermal conductivity of the carbon nanotube are as follows:

$$\begin{aligned} \bar{\rho}_{nf} &= \rho_f \left(1 - \phi + \phi \left(\frac{\rho_{CNT}}{\rho_f} \right) \right), \tilde{\mu}_{nf} = \frac{1}{(1 - \phi)^{2.5}}, \\ \tilde{\alpha}_{nf} &= (1 - \phi)(\rho_f)_f + \phi(\rho_s)_{CNT}, \\ (\rho c_p)_{nf} &= (1 - \phi)(\rho c_p)_f + \phi(\rho c_p)_{CNT}, \\ k_{nf} &= \frac{1 - \phi + 2\phi \left(\frac{k_{CNT}}{k_f} \right) \ln \left(\frac{k_{CNT} + k_f}{2k_f} \right)}{1 - \phi + 2\phi \left(\frac{k_f}{k_{CNT} - k_f} \right) \ln \left(\frac{k_{CNT} + k_f}{2k_f} \right)}. \end{aligned}$$

Due to the magnetic dipole, the assumed liquid flow is affected by the magnetic field, whose magnetic scalar potential is given by (Everts et al., 2020; Reddy et al., 2022)

$$\begin{aligned} \phi_1 &= \frac{\gamma}{2\pi} \left[\frac{x}{x^2 + (y+a)^2} \right], H_x = -\frac{\partial \phi_1}{\partial x} \\ &= \frac{\gamma}{2\pi} \left\{ \frac{x^2 - (y+a)^2}{[x^2 - (y+a)^2]^2} \right\} \text{ and } H_y = -\frac{\partial \phi_1}{\partial y} \\ &= \frac{\gamma^*}{2\pi} \left\{ \frac{2x(y+a)}{[x^2 - (y+a)^2]^2} \right\}. \end{aligned}$$



where

$$H = \left[\left(\frac{\partial \phi_1}{\partial x} \right)^2 + \left(\frac{\partial \phi_1}{\partial y} \right)^2 \right]^{\frac{1}{2}} \tag{9}$$

From Eq. 9, one can get

$$\frac{\partial}{\partial x} H = -\frac{\gamma}{2\pi} \left(\frac{2x}{(y+a)^4} \right),$$

$$\frac{\partial}{\partial x} H = -\frac{\gamma}{2\pi} \left(\frac{2}{(y+a)^3} + \frac{4x^2}{(y+a)^5} \right)$$

We assume that the applied field H is sufficiently strong to saturate the assumed fluid and the variation of magnetization M with temperature T is approximated by the linear equation

$$M = K(T_c - T).$$

where K indicates the gyromagnetic coefficient. We establish the below transformations to lessen the dimensions of the above equation to 1

$$\tilde{u} = bx f'(\eta), \tilde{v} = -\sqrt{bv_f} f(\eta), \tilde{u}_p = bx F'(\eta), \tilde{v}_p = -\sqrt{bv_f} F(\eta),$$

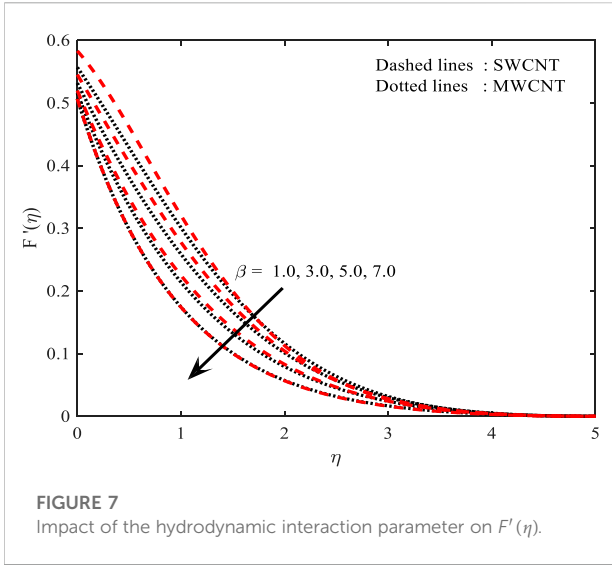


FIGURE 7
Impact of the hydrodynamic interaction parameter on $F'(\eta)$.

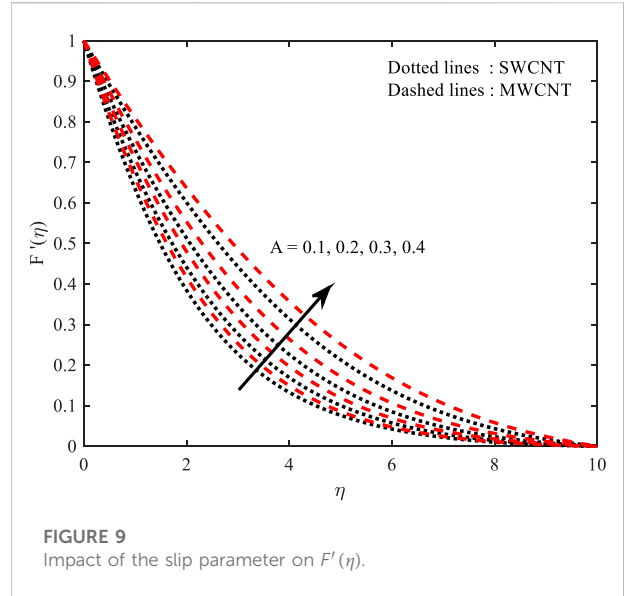


FIGURE 9
Impact of the slip parameter on $F'(\eta)$.

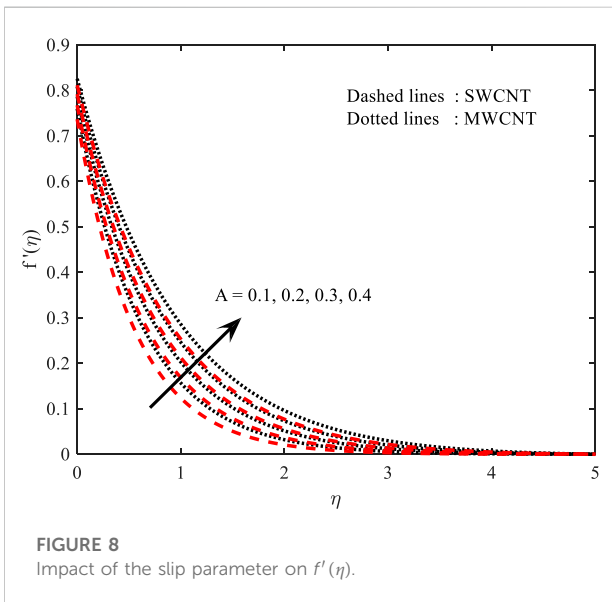


FIGURE 8
Impact of the slip parameter on $f'(\eta)$.

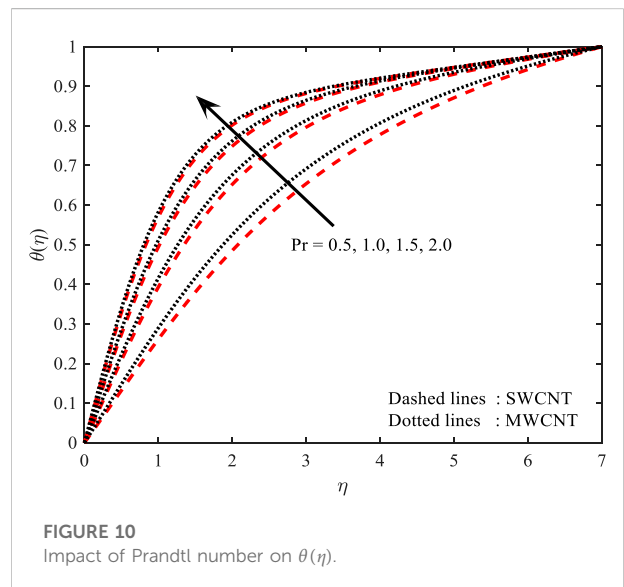


FIGURE 10
Impact of Prandtl number on $\theta(\eta)$.

$$\eta = \sqrt{\frac{b}{\nu_f}} y, \theta(\eta) = \frac{T - T_w}{T_w - T_\infty}, \theta_p(\eta) = \frac{T_p - T_w}{T_w - T_\infty}. \quad (10)$$

On employing the above, Eqs 1, 4 are satisfied identically, and Eqs 2, 3, 5, 6 reduce as

Fluid phase:

$$f''' + \frac{1}{(1-\phi)^{2.5} \left(1 - \phi + \phi \left(\frac{\rho_s}{\rho_f} \right)_{CNT} \right)} (f f'' - f'^2) - \frac{2\beta\theta}{\rho_f(\eta+\gamma)^4} + [(1-\phi)^{2.5}] [l\beta_v(F' - f')] = 0 \quad (12)$$

$$\frac{k_{mf}}{k_f} \theta'' + \text{Pr} \left(1 - \phi + \phi \left(\frac{\rho c_p}{\rho c_p} \right)_{CNT} \right) f \theta' - \frac{2\beta(\theta - \varepsilon)f}{(\eta + \gamma)^3} + \frac{\text{Pr}l\beta_t}{m} [\theta_p - \theta] + \text{Pr}l\beta_v Ec [F' - f']^2 = 0, \quad (13)$$

Dust phase:

$$FF'' - F'^2 + \beta_v [f' - F'] = 0, \quad (14)$$

$$F\theta'_p + \gamma\beta_t [\theta - \theta_p] = 0 \quad (15)$$

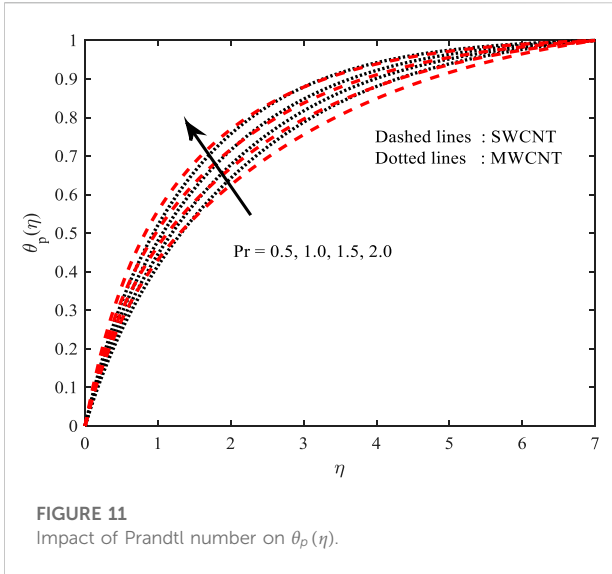


FIGURE 11
Impact of Prandtl number on $\theta_p(\eta)$.

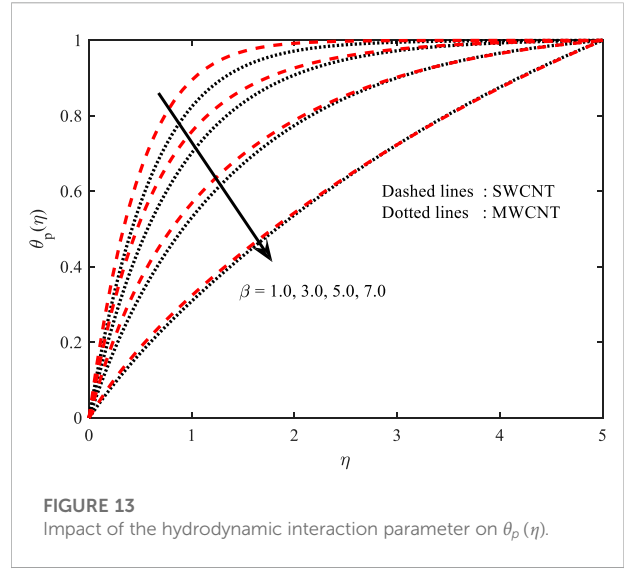


FIGURE 13
Impact of the hydrodynamic interaction parameter on $\theta_p(\eta)$.

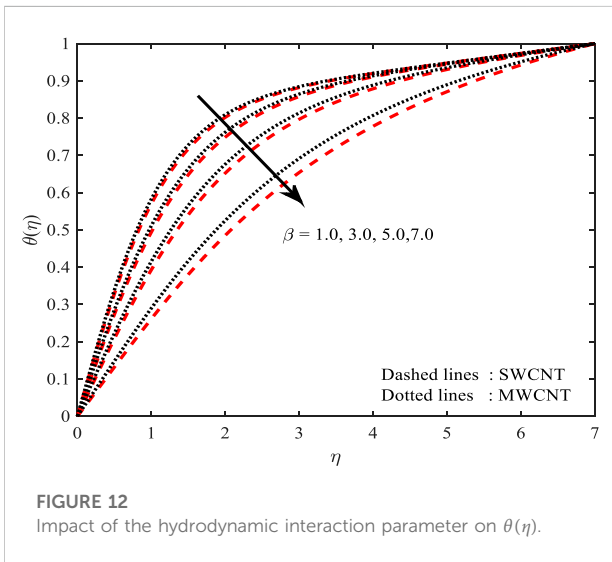


FIGURE 12
Impact of the hydrodynamic interaction parameter on $\theta(\eta)$.

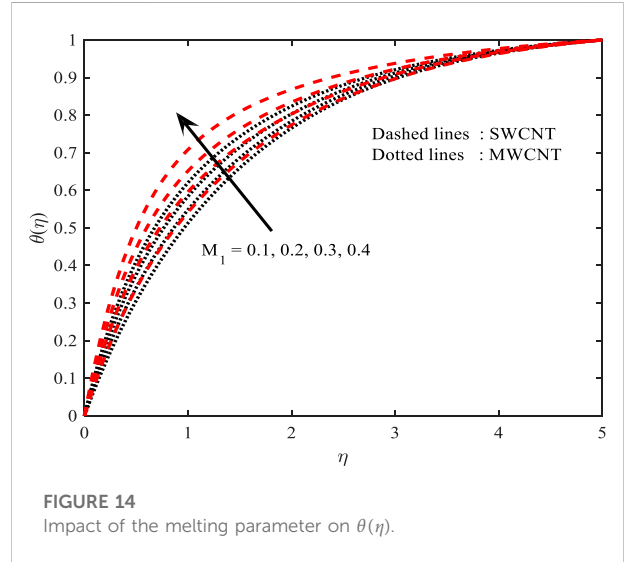


FIGURE 14
Impact of the melting parameter on $\theta(\eta)$.

Reduced boundary conditions:

$$\begin{aligned} Pr f(0) + M_1 \theta(0) &= 0, f'(0) = 1 + A f''(0), \theta(0) = 0 \\ f'(\infty) &= 0, F'(\infty) = 0, F(\infty) = f(\infty), \theta(\infty) = 0, \theta_p(\infty) \\ &= 0. \end{aligned} \tag{16}$$

The skin friction coefficient and Nusselt number are defined as

$$C_f = \left(1 + \frac{1}{\beta}\right) \frac{\tau_w}{\rho_f u_w^2}, Nu_x = \frac{q_w u_w}{b k_{nf} (T_f - T_\infty)} \frac{\partial T}{\partial y},$$

The transformed form of the above one is

$$\sqrt{Re_x} C_f = \left(1 + \frac{1}{\beta}\right) \frac{1}{(1 - \phi)^{2.5}} f''(0), \frac{Nu_x}{\sqrt{Re_x}} = -\frac{k_{nf}}{k_f} \theta'(0),$$

The following are the dimensionless parameters that exist in the problem:

$$\begin{aligned} \beta &= \frac{\gamma}{2\pi} \frac{\mu_0 K (T_c - T_w) \rho}{\mu^2}, \beta_v = \frac{1}{b \tau_v}, \gamma = \sqrt{\frac{S P c^2}{\mu}}, Pr = \frac{1}{b \tau_t}, Ec \\ &= \frac{\tilde{U}_w^2}{c_p (T_w - T_\infty)}, M_1 = \frac{C_f (T_\infty - T_m)}{\lambda + C_s (T_m - T_0)}, A = k_1 \sqrt{\frac{b}{\nu}} \text{ and,} \\ Re_x &= \frac{u_w^2}{b \nu_f}. \end{aligned}$$

Numerical procedure

The reformed system of coupled nonlinear ODEs (Eqs 12–15) in conjunction with boundary conditions (Eq. 16) is

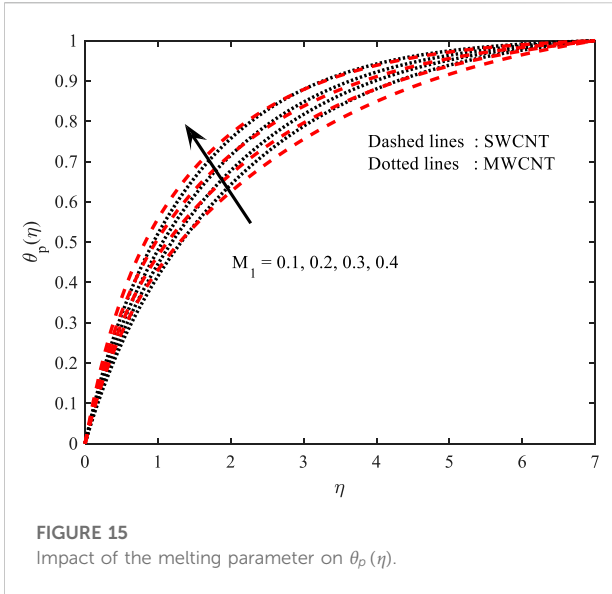


FIGURE 15 Impact of the melting parameter on $\theta_p(\eta)$.

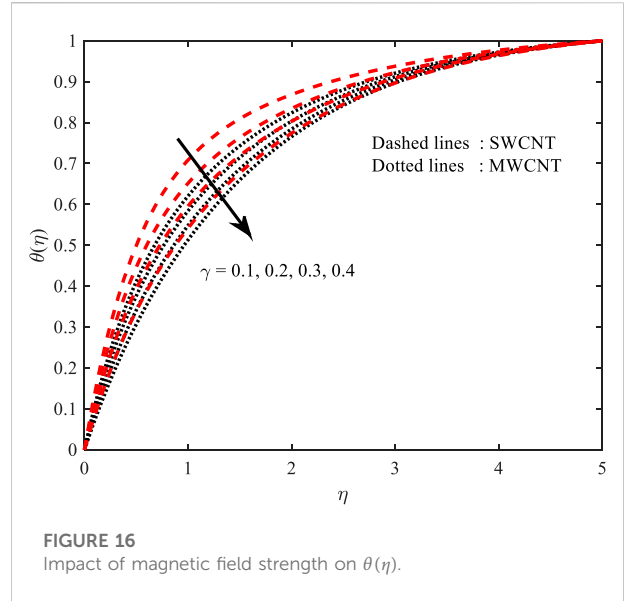


FIGURE 16 Impact of magnetic field strength on $\theta(\eta)$.

worked out for various parameters by employing the tool of MATLAB function bvp4c. It is an efficient method used by several authors to tackle such problems. A fair amount of computations are executed by using the tool mentioned above, so to deal with it, we considered $[0; \eta_{\max}]$ as a domain in place of $[0; 1)$, where η_{\max} is an appropriate real number, as the results are not altered for $\eta > \eta_{\max}$. Authentication of the accuracy of the numerical procedure used was done by comparison first; computations for $f''(0)$ are carried out for the viscous fluid for various values of β and compared with the available published results as shown in Table 1, and they establish an excellent agreement.

Fluid phase

$$f = y_1, f' = y_2, f'' = y_3, F = y_4, F' = y_5$$

$$\theta = y_6, \theta' = y_7, \theta_p = y_8$$

$$y_3' = - \left[\frac{1}{(1-\phi)^{2.5} \left(1 - \phi + \phi \left(\frac{\rho_p}{\rho_f} \right)_{CNT} \right)} (y_1 y_3 - y_2^2) - \frac{2\beta\theta}{\rho_f(\eta + \gamma)^4} + [(1-\phi)^{2.5}] [l\beta_v(y_5 - y_2)] \right] \tag{17}$$

$$y_7' = - \frac{1}{k_{mf}} \left[\text{Pr} \left(1 - \phi + \phi \left(\frac{\rho c_p}{\rho c_p} \right)_{CNT} \right) y_1 y_7 - \frac{2\beta(y_6 - \varepsilon)y_1}{(\eta + \gamma)^3} + \frac{\text{Pr}l\beta_t}{m} [y_8 - y_6] \right] - \frac{1}{k_{mf}} [\text{Pr}l\beta_v Ec [y_5 - y_2]^2] \tag{18}$$

Dust phase

$$y_5' = \frac{1}{y_4} [y_5' - \beta_v [y_2 - y_5]] \tag{19}$$

$$y_8' = - \frac{1}{y_4} [y\beta_t [y_6 - y_8]] \tag{20}$$

Reduced boundary conditions:

$$\text{Pr} y_1(0) + M_1 y_6(0) = 0, \quad y_2(0) = 1 + A y_3(0), \quad y_6(0) = 0$$

$$y_2(\infty) = 0, \quad y_5(\infty) = 0, \quad y_4(\infty) = y_1(\infty), \quad y_6(\infty) = 0, \quad y_8(\infty) = 0 \tag{21}$$

Results and discussion

In the present article, the investigation is carried out on the significance of magnetic dipole flow and melting heat transfer over suspended dust particles and carbon nanotubes. Table 2 represents the mathematical form of transport characteristics of the nanofluid. The computation for the various profiles is deliberated via graphs, whereas the rate quantities' numerical results are displayed in a tabular form (Table 3).

Velocity profile ($f'(\eta)$ and $F'(\eta)$)

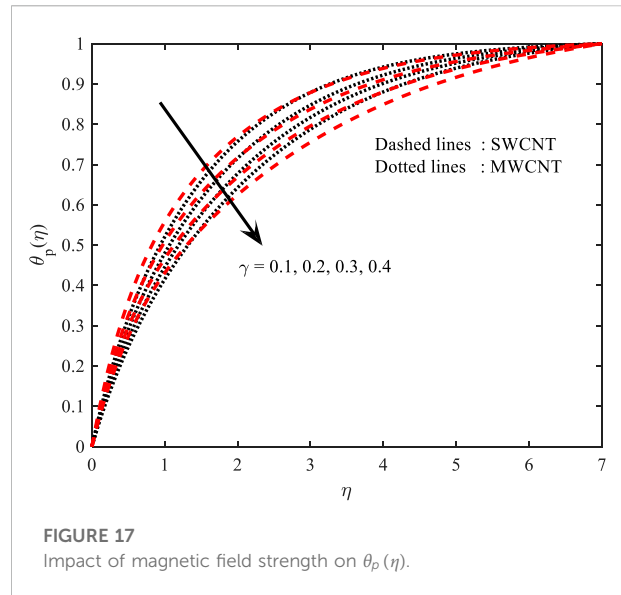
The magnetic field strength (γ) parameter has a significant influence on the induced magnetism, as shown in Figures 2, 3. It is perceived in Figure 2 that an expansion in the field strength of the magnetic (γ) parameter leads to a decline in the velocity of the fluid phase ($f'(\eta)$). This is

because an increment in γ is directly proportional to Lorentz forces at the surface. This is a resistive type of force that declines the fluid velocity and the magnetic field intensity. Magnetic field strength (γ) parameters have a terrific control on the velocity profile for the dusty phase [$F'(\eta)$], as illustrated in Figure 4. This numerical rise in γ ($= 0.1, 0.3, 0.5, 0.7$) represents a consequent reduction in the velocity profile for the dusty phase. Consequently, the inner thickness of the boundary layer also scales back for larger γ . Furthermore, we can observe that the performance velocity profile in the MWCNT case is more efficient than that of the SWCNT case.

In Figures 4, 5, the behavior of ϕ on the velocity of both $f'(\eta)$ and $F'(\eta)$ phases was highlighted. A higher amount of nanoparticles sufficiently enhances the velocity of the fluid for both $f'(\eta)$ and $F'(\eta)$ phases. Besides, the complementary circumscription layer has been appreciated for strengthening the numerical values of ϕ . Additionally, the fluid flow of the MWCNT case is higher than the velocity of the fluid flow of SWCNT. The upshot of β (hydrodynamic interaction parameter) on velocity distribution on both $f'(\eta)$ and $F'(\eta)$ cases are observed in Figures 6, 7. A significant escalation in the β parameter causes a decrement in both $f'(\eta)$ and $F'(\eta)$ phases, which leads to scale down the fluid at the circumscription layer. Furthermore, the complementary circumscription momentum layer also dismisses both $f'(\eta)$ and $F'(\eta)$ phases for esteemed values of β . Additionally, the fluid flow velocity in MWCNT is much more than that of the fluid flow velocity of SWCNT. Figures 8, 9 illustrate the dimensionless velocity profiles for both $f'(\eta)$ and $F'(\eta)$ cases over variant values of emerging parameter A . These figures show that both $f'(\eta)$ and $F'(\eta)$ enhance booming values of A . Likewise, the complementary circumscription thermal layer rises for both $f'(\eta)$ and $F'(\eta)$ by thicker values of A .

Temperature profile ($\theta(\eta)$ and $\theta_p(\eta)$)

Figures 10, 11 portray the performance of the Prandtl number on the thermal gradient for both $\theta(\eta)$ and $\theta_p(\eta)$ phases. It shows an improvement in the temperature distribution of both $\theta(\eta)$ and $\theta_p(\eta)$ for bulkier numerical values of Pr . This is the consequence of enhanced thermal layer thickness. The heat-transfer rate increases because of the temperature gradient at the boundary. Additionally, the complementary circumscription thermal layer is also predominant for greater values of Pr . Here, we can observe that the efficiency of fluid temperature is more in the SWCNT case than in the MW CNT case. Figures 12, 13 represent the analogous behaviors of β (hydrodynamic interaction parameter) on temperature fields for both $\theta(\eta)$ and $\theta_p(\eta)$ phases. They are both critical functions of β . Meanwhile, the



thickness of boundary layers of temperature becomes thinner for amplified β . Additionally, the MWCNT case dominates the fluid temperature more than the SWCNT case. The thermal gradient structure expands with advancing values of M_1 as showcased in Figures 14, 15 for both $\theta(\eta)$ and $\theta_p(\eta)$ cases. Here, the melting parameter has a direct relation with the thermal gradient and for preponderant values of M_1 heightens the temperature gradient for both (η) and $\theta_p(\eta)$ cases. Likewise, the complementary circumscription thermal layer also has an upsurge for hiking values of M_1 . Meanwhile, the SWCNT case has a higher impact on fluid temperature when treated with the MWCNT case. The temperature gradient nature is portrayed in Figures 16, 17 for the various γ parameters. It is noted that the assessable rise in (γ) shows a remarkable decrement in the temperature distribution for both $\theta(\eta)$ and $\theta_p(\eta)$ cases. Likewise, there is circumscription thermal layer shrinkage for hiking values of γ . Meanwhile, the MWCNT case has a higher impact on fluid temperature when treated with the SWCNT case.

Numerical outcomes of $Re_x^{1/2}C_f$ and $Re_x^{1/2}Nu_x$ friction factors are shown in Table 3. In the table, we analyzed that when enlarging the values of parameters β, β_1, ϕ_1 and M_1 , $Re_x^{1/2}C_f$ shows thicker behavior, while the hiking values of the exact parameter show opposite behavior for $Re_x^{1/2}Nu_x$. Furthermore, $Re_x^{1/2}Nu_x$ heightens for booming values of Pr and β_t .

Conclusion

This research work inspected the significance of magnetic dipole flow and melting heat transfer over suspended dust

particles. The impact of melting is also discussed in the energy equation. Fluid flow and the heat-transfer rate are discussed through a mathematical model of second-order, nonlinear ODEs, which is analyzed numerically. The effectiveness of appropriate parameters is elaborated graphically. The impacts of essential parameters are reported.

- The velocity field declined against the impact of γ parameter.
- The velocity of the fluid increases with higher estimations of ϕ .
- The fluid temperature decays with a bulkier assessment of β .
- Because of melting, the thermal field is more for the rising assessment of Pr .
- On enlarging the values of parameters β and M_1 , $Re_x^{1/2}C_f$ shows thicker behavior.
- $Re_x^{1/2}Nu_x$ heightens for booming values of Pr and β_1 .
- The velocity field is dramatically shortened with higher β .
- The slip parameter plays a significant role in enhancing the velocity profile.

Data availability statement

The raw data supporting the conclusion of this article will be made available by the authors, without undue reservation.

References

- Alkanhal, T. A., Sheikholeslami, M., Usman, M., Rizwan, ul Haq, Shafeeg, Ahmad, Abdullah, S.-A., et al. (2019). Thermal management of MHD nanofluid within the porous medium enclosed in a wavy shaped cavity with square obstacle in the presence of radiation heat source. *Int. J. Heat Mass Transf.* 139, 87. doi:10.1016/j.ijheatmasstransfer.2019.05.006
- Bilal, M., Sagheer, M., and Hussain, S. (2018). Numerical study of magnetohydrodynamics and thermal radiation on Williamson nanofluid flow over a stretching cylinder with variable thermal conductivity. *Alexandria Eng. J.* 57, 3281–3289. doi:10.1016/j.aej.2017.12.006
- Chen, C. K., Chen, B. S., and Liu, C. C. (2015). Entropy generation in mixed convection magnetohydrodynamic nanofluid flow in vertical channel. *Int. J. Heat Mass Transf.* 91, 1026–1033. doi:10.1016/j.ijheatmasstransfer.2015.08.042
- Choi, S. U. S. (1995). *Enhancing thermal conductivity of fluids with nanoparticles, developments and applications of non-Newtonian flows*, 231. New York: ASME, 99–105.
- Choi, S. U. S., Zhang, Z. G., Yu, W., Lockwood, F. E., and Grulke, E. A. (2001). Anomalous thermal conductivity enhancement in nanotube suspensions. *Appl. Phys. Lett.* 79, 2252–2254. doi:10.1063/1.1408272
- Dogonchi, A. S., and Ganji, D. D. (2016). Investigation of MHD nanofluid flow and heat transfer in a stretching/shrinking convergent/divergent channel considering thermal radiation. *J. Mol. Liq.* 220, 592–603. doi:10.1016/j.molliq.2016.05.022
- Everts, M., Bhattacharyya, S., Bashir, A. I., and Meyer, J. P. (2020). Heat transfer characteristics of assisting and opposing laminar flow through a vertical circular tube at low Reynolds numbers. *Appl. Therm. Eng.* 179, 115696. doi:10.1016/j.applthermaleng.2020.115696
- Fakour, M., Vahabzadeh, A., and Ganji, D. D. (2015). Study of heat transfer and flow of nanofluid in permeable channel in the presence of magnetic field. *Propuls. Power Res.* 4, 50–62. doi:10.1016/j.jprr.2015.02.005
- Hashemi, H., Namazian, Z., Zadeh, S. M. H., and Mehryan, S. A. M. (2018). MHD natural convection of a micropolar nanofluid flowing inside a radiative porous medium under LTNE condition with an elliptical heat source. *J. Mol. Liq.* 271, 914–925. doi:10.1016/j.molliq.2018.09.010
- Hayat, T., Aslam, N., Khan, M. I., Khan, M. I., and Alsaedi, A. (2019). Physical significance of heat generation/absorption and Soret effects on peristalsis flow of pseudoplastic fluid in an inclined channel. *J. Mol. Liq.* 275, 599–615. doi:10.1016/j.molliq.2018.11.055
- Hayat, T., Khan, M. I., Farooq, M., Yasmeen, T., and Alsaedi, A. (2016). Water-carbon nanofluid flow with variable heat flux by a thin needle. *J. Mol. Liq.* 224, 786–791. doi:10.1016/j.molliq.2016.10.069
- Hayat, T., Muhammad, T., Shehzad, S. A., and Alsaedi, A. (2017). An analytical solution for magnetohydrodynamic Oldroyd-B nanofluid flow induced by a stretching sheet with heat generation/absorption. *Int. J. Therm. Sci.* 111, 274–288. doi:10.1016/j.ijthermalsci.2016.08.009
- Hayat, T., and Nadeem, S. (2017). Heat transfer enhancement with AgCuO/water hybrid nanofluid. *Results Phys.* 7, 2317–2324. doi:10.1016/j.rinp.2017.06.034
- Hayat, T., Rashid, M., Khan, M. I., and Alsaedi, A. (2018). Melting heat transfer and induced magnetic field effects on flow of water based nanofluid over a rotating disk with variable thickness. *Results Phys.* 9, 1618–1630. doi:10.1016/j.rinp.2018.04.054
- Hayat, T., Sajjad, R., Ellahi, R., Alsaedi, A., and Muhammad, T. (2017). Homogeneous-heterogeneous reactions in MHD flow of micropolar fluid by a curved stretching surface. *J. Mol. Liq.* 240, 209–220. doi:10.1016/j.molliq.2017.05.054
- Hayat, T., Shehzad, S. A., and Qasim, M. (2013). Slip effects on the unsteady stagnation point flow with variable free stream. *Walaialk J.* 10, 385–394.
- Kumar, K. G., Gireesha, B. J., Rudraswamy, N. G., and Krishnamurthy, M. R. (2019). An unsteady flow and melting heat transfer of a nanofluid over a stretching

Author contributions

HA: conceptualization, methodology, validation, investigation, resources, data curation, writing—original draft, writing—review and editing, visualization, and supervision.

Funding

This work was supported by the Deanship of Scientific Research, Vice Presidency for Graduate Studies and Scientific Research, King Faisal University, Saudi Arabia (Project No. GRANT639).

Conflict of interest

The author declares that the research was conducted in the absence of any commercial or financial relationships that could be construed as a potential conflict of interest.

Publisher's note

All claims expressed in this article are solely those of the authors and do not necessarily represent those of their affiliated organizations or those of the publisher, the editors, and the reviewers. Any product that may be evaluated in this article or claim that may be made by its manufacturer is not guaranteed or endorsed by the publisher.

sheet embedded in a porous medium An Unsteady Flow and Melting Heat Transfer of a Nanofluid over a Stretching Sheet Embedded in a Porous Medium. *Int. J. Appl. Mech. Eng.* 24 (2), 245–258. doi:10.2478/ijame-2019-0016

Mahanthesh, B., Gireesha, B. J., and Gorla, R. S. R. (2017). Unsteady three-dimensional MHD flow of a nano Eyring-Powell fluid past a convectively heated stretching sheet in the presence of thermal radiation, viscous dissipation and Joule heating. *J. Assoc. Arab Univ. Basic Appl. Sci.* 23, 75–84. doi:10.1016/j.jaubas.2016.05.004

Mukhopadhyay, S. (2013). MHD boundary layer slip flow along a stretching cylinder. *Ain Shams Eng. J.* 4, 317–324. doi:10.1016/j.asej.2012.07.003

Pourmehran, O., Gorji, M. R., and Ganji, D. D. (2016). Heat transfer and flow analysis of nanofluid flow induced by a stretching sheet in the presence of an external magnetic field. *J. Taiwan Inst. Chem. Eng.* 65, 162–171. doi:10.1016/j.jtice.2016.04.035

Qayyum, S., Hayat, T., and Alsaedi, A. (2017). Chemical reaction and heat generation/absorption aspects in MHD nonlinear convective flow of third grade nanofluid over a nonlinear stretching sheet with variable thickness. *Results Phys.* 7, 2752–2761. doi:10.1016/j.rinp.2017.07.043

Ramesh, G., Gireesha, B., Bagewadi, C., Ramesh, G. K., Gireesha, B. J., and Bagewadi, C. S. (2012). MHD flow of a dusty fluid near the stagnation point over a permeable stretching sheet with non-uniform source/sink. *Int. J. Heat Mass Transf.* 55 (17–18), 4900–4907. doi:10.1016/j.ijheatmasstransfer.2012.05.003

Reddy, G. J., Kethireddy, B., Kumar, M., and Hoque, M. M. (2018). A molecular dynamics study on transient non-Newtonian MHD Casson fluid flow dispersion over a radiative vertical cylinder with entropy heat generation. *Journal of Molecular Liquids* 252, 245–262. doi:10.1016/j.molliq.2017.12.077

Reddy, M. G., Sudharani, M., Praveena, M. M., and Kumar, K. G. (2022). Effect of thermal conductivity on Blasius-Rayleigh-Stokes flow and heat transfer over a moving plate by considering magnetic dipole moment. *Eur. Phys. J. Plus* 137 (1), 1–13. doi:10.1140/epjp/s13360-021-02259-1

Reddy, M. G., and Kumar, K. G. (2021). Cattaneo-christov heat flux feature on carbon nanotubes filled with micropolar liquid over a melting surface: A stream line study Cattaneo-christov heat flux feature on carbon nanotubes filled with

micropolar liquid over a melting surface: A stream line study. *Int. Commun. Heat Mass Transf.* 122, 105142. doi:10.1016/j.icheatmasstransfer.2021.105142

Rizwan, U. H., Raza, A., Ebrahim, A. A., and Iskander, T. (2020). Heat transfer analysis of water based SWCNTs through parallel fins enclosed by square cavity. *Int. Commun. Heat Mass Transf.* 119, 104797. doi:10.1016/j.icheatmasstransfer.2020.104797

Rizwan Ul Haq, S., Naveed, K., and Toufik, M. (2017). Thermal management of water-based SWCNTs enclosed in a partially heated trapezoidal cavity via FEM. *Int. J. Heat Mass Transf.* 112, 972. doi:10.1016/j.ijheatmasstransfer.2017.05.041

Sheikholeslami, M. (2017). Lattice Boltzmann method simulation for MHD non-Darcy nanofluid free convection. *Phys. B Condens. Matter* 516, 55–71. doi:10.1016/j.physb.2017.04.029

Sheikholeslami, M., Shehzad, S. A., and Li, Z. (2018). Nanofluid heat transfer intensification in a permeable channel due to magnetic field using Lattice Boltzmann method. *Phys. B Condens. Matter* 542, 51–58. doi:10.1016/j.physb.2018.03.036

Shen, M., Wang, F., and Chen, H. (2015). MHD mixed convection slip flow near a stagnation-point on a nonlinearly vertical stretching sheet. *Bound. Value Probl.* 78, 2015. doi:10.1186/s13661-015-0340-6

Ul Haq, R., Rashid, I., Khan, Z., Rashid, I., and Khan, Z. H. (2017). Effects of aligned magnetic field and CNTs in two different base fluids over a moving slip surface. *J. Mol. Liq.* 243, 682–688. doi:10.1016/j.molliq.2017.08.084

Ul Haq, R., Raza, A., Algehyne, E. A., and Iskander, T. (2020). Dual nature study of convective heat transfer of nanofluid flow over a shrinking surface in a porous medium. *Int. Commun. Heat Mass Transf.* 114, 104583. doi:10.1016/j.icheatmasstransfer.2020.104583

Ul Haq, R., Soomro, F. A., Hammouch, Z., and Ur Rehman, S. (2018). Heat exchange within the partially heated C-shape cavity filled with the water based SWCNTs. *Int. J. Heat Mass Transf.* 127, 506–514. doi:10.1016/j.ijheatmasstransfer.2018.07.101

Zhao, G., Wang, Z., and Jian, Y. (2019). Heat transfer of the MHD nanofluid in porous microtubes under the electrokinetic effects. *Int. J. Heat Mass Transf.* 130, 821–830. doi:10.1016/j.ijheatmasstransfer.2018.11.007

Nomenclature

A velocity slip parameter

β Hydrodynamic interaction parameter

β_v fluid–particle interaction for velocity

β_t fluid–particle interaction for temperature

c_{pf} specific heat of fluid particles

c_{mf} specific heat of dust particles

Ec Eckert number

k_1 slip constant

λ_0 magnetic permeability

MWCNT multiwall carbon nanotube

μ_{nf} viscosity of carbon nanotubes

M_1 melting parameter

N density of dust particles

Pr Prandtl number

ϕ volume fraction of the nanoparticle parameter

Re_x local Reynolds number

ρ_{nf} density of carbon nanotubes

SWCNT single-wall carbon nanotube

T, T_p temperature of the fluid and dust phases

τ_v relaxation time for the dust particle

T_w wall temperature

T_∞ ambient fluid temperature

\tilde{u}, \tilde{u}_p velocity components along the x -axis

U_w wall velocity

\tilde{v}, \tilde{v}_p velocity components along the y -axis

γ magnetic field strength